Journal of Innovative Materials in Extreme Conditions 2024 Volume 5 Issue 2

UV-VIS TRANSMITTANCE AND BAND GAP OF ZINC OXIDE FILMS PREPARED BY FEMTOSECOND PULSE-LASER-DEPOSITION

Dieter Fischer[1]*, and Dejan Zagorac[2]

[1]*Max Planck Institute for Solid State Research, Heisenbergstr. 1, 70569 Stuttgart, Germany*

[2]*Institute of Nuclear Sciences Vinca, Materials Science Laboratory, University of Belgrade, Belgrade, Serbia*

Corresponding author*: d.fischer@fkf.mpg.de

[$]Dedicated to J. Christian Schön on the occasion of his 66th birthday

Abstract: *The zinc oxide thin films were deposited on sapphire substrates using the femtosecond pulsed-laser-deposition method in the temperature range of -190 to 200 °C. The Ultraviolet-Visible Spectroscopy (UV-VIS) transmittance of the ZnO films was recorded between 200 nm and 800 nm and the films showed an unexpected behavior below 380 nm. In addition, band structure calculations of the ZnO supercell models were performed using a hybrid B3LYP functional. Furthermore, a novel hypothetical ZnO_2 structure was optimized using HSE functional and its band structure was also calculated to provide a possible explanation for the experimental measurements of the deposited ZnO films. The anomalous transmittance of the ZnO films subsequent to the absorption edge down to 200 nm, can be attributed to the presence of dioxygen species in the films. This conclusion is supported by the calculated band structures of a relaxed-distorted ZnO structure and a novel constructed ZnO_2 structure, both of which contain dioxygen species.*

Keywords: *zinc oxide, thin films, UV/VIS transmittance, band structure calculations, superoxide ions*

1. Introduction

Zinc oxide (ZnO) is a direct semiconductor with a wide bandgap of 3.4 eV and a large exciton binding energy of 60 meV at room temperature.[1] The electronic band structure has been calculated by many groups. The results of the band structure calculation using LDA with SIC-PP determine the band gap to 3.77 eV. [2] Due to the diverse applications of ZnO, e.g. as a transparent conductive film, sensor, and detector, a precise knowledge of the band structure is crucial for determining its potential utility. In this context, several theoretical approaches with varying degrees of complexity have been used to calculate the band structure of ZnO. Thus, ZnO has been investigated for various crystal structures, [3, 4] doping [5, 6] and the influence of intrinsic point defects [7] and cation/anion exchange in bulk,[8] core-shell,[9] nanostructures,[10] and monolayers of ZnO for nanoscale electronic [11] and optoelectronic properties [12] and for advanced thermoelectric applications.[13] However, none of these studies included the presence dioxygen species in ZnO.

From an experimental point of view, polycrystalline films of ZnO (40 nm thick) prepared by pulsed laser deposition (PLD) show a slightly smaller bandgap of about 3.2 eV compared to the bulk material as well as an additional absorption band (excitons) at around 3.5 eV.[14] The excitonic structure was studied in detail on epitaxial ZnO films, which were also prepared by PLD.[15] Furthermore, the doping of ZnO films with Al [10] and the formation of ZnO/(Zn, Mg)O multilayers [16] leads to a blue shift of the bandgap up to about 3.6 eV. In addition to the PLD process, many other methods have been used to grow ZnO films. We will only mention a few of them here to show the possible variations that have been achieved. Pure ZnO films prepared by spray pyrolysis also have a band gap of around 3.3 eV.[17] Pure

ZnO films [18], and Ga and Ag-doped ZnO films [19, 20] prepared by the sol-gel method lead to bandgaps between 3.2 and 3.4 eV. A solution-based synthesis of ZnO films containing a complexing agent leads to a bandgap of 3.75 eV [18]. Very high or low band energies were reported for ZnO-based alloyed systems adapting the wurtzite structure with $Mg_xZn_{1-x}O$, 4.3 eV, and $Cd_xZn_{1-x}O$, 2.5 eV, respectively (all prepared by PLD). However, transmittances in the range of 5 eV or higher (<250 nm) have never been observed. [21] In contrast, the ZnO films described here have a transmittance in this range.

2. Experimental Methods

The ZnO films were deposited on epi-polished, single-crystal sapphire substrates (orientation (0001), CrysTec GmbH, Germany) using a femtosecond laser system (FemtoRegen, High-Q-Laser GmbH, Austria) with a wavelength of 516 nm at 442 femtosecond. The PLD target used was prepared by pressing ZnO powder (99.999 %, lightly yellow, Acros Organics, Belgium) with 8 tons of pressure in an argon atmosphere forming a round disc (diameter: 16 mm). The depositions were performed in a vacuum chamber with a process pressure of $6\text{-}8x10^{-8}$ mbar for a period of 6-7 hours per sample; further details are given in [22]. During the deposition, the substrate temperature was kept constant at -190, 25, 100, and 200 °C on a copper sample holder, which is connected to a transfer cart system. The copper holder contains a resistance heater including a PT-100 thermal sensor and is connected to two pipes, which allow the cooling by a liquid nitrogen flow through the holder. After deposition, the samples were transferred under vacuum and stored in a glove box in an argon atmosphere.

The scanning electron microscope (SEM) images were recorded with a field-emission microscope (Merlin, Zeiss GmbH, Germany) using an accelerating voltage of 5 kV and an in-lens detector. The samples were transferred into the microscope in an argon atmosphere using a custom-built transfer chamber.

The transmission spectra (wavelength range 200 to 800 nm) of the films were measured by a UV/VIS/NIR-spectrometer (Lambda 9, Perkin-Elmer, USA) directly on the substrates at ambient conditions containing a slit of 6 mm. The plotted transmission spectra are comparable because all films have been prepared under analogous conditions. Due to the different film thicknesses, the transmission spectra were not normalized.

3. Theoretical Methods

The investigated ZnO structures were generated using 2x2x2 supercells in which oxygen ions were replaced by dioxygen species and in which one oxygen atom was moved from a regular occupied tetrahedral position to an inverse tetrahedral void, and as an ideal ZnO wurtzite structure [23, 24]. The *ab initio* calculations were performed using the CRYSTAL17 code, based on the linear combination of atomic orbitals. [25] The local optimizations of structures employed analytical gradients and the subsequent phonon calculations were based on analytical first and numerical second derivatives. [26]

Band structure calculations were performed on the density functional theory (DFT) level, employing the B3LYP functional (Becke's three-parameter functional in combination with the correlation functional of Lee, Yang, and Parr) in the case of ZnO phases. [27] In addition, we employed a hybrid HSE (Heyd–Scuseria–Ernzerhof) approach for ZnO_2, [28] because it is important to use several different *ab initio* methods, to get some feeling for the quantitative validity of the results. [29, 30] Each calculation employed an all-electron basis set (AEBS): a [6s5p2d] basis set in the case of zinc, and a [4s3p] basis set

in the case of oxygen. [31] In each structural optimization, Fock/KS matrix mixing was set to 30%, and the tolerances for the convergence on energy were set to 10^{-7}. K-point meshes of 8 x 8 x 8 Monkhorst-Pack scheme have been used. Structural and crystallographic analysis has been performed using the KPLOT package. [32] ZnO_2 structure was visualized using VESTA code. [33]

4. Results and Discussion

The ZnO films were deposited on sapphire substrates at temperatures of -190, 25, 100, and 200 °C using the femtosecond pulsed-laser-deposition method. The obtained rough, dense films are 60 to 100 nm thick and show a granular surface structure with particle sizes between 10 and 50 nm. In addition, some droplets in the micrometer range can be seen in the SEM images. The SEM images of the different ZnO films are shown in Fig.1. Remarkable is the variation of the color of the films obtained for different substrate temperatures. The films deposited at -190 and 200 °C are colorless and at 25 and 100 °C they are gray-yellow. The gray color is caused by the segregation of zinc and the yellow color corresponds to the presence of superoxide ions in these films. The origin of this behavior is the presence of dioxygen species (such as O_2^-, O_2^{2-}, O_2, …), which occur in all ZnO films due to the occupation of adjacent, face-connected tetrahedral voids within the hexagonal close-packed zinc lattice. The yellow superoxide ion is then formed at around room temperature in the films (cf. [22]).

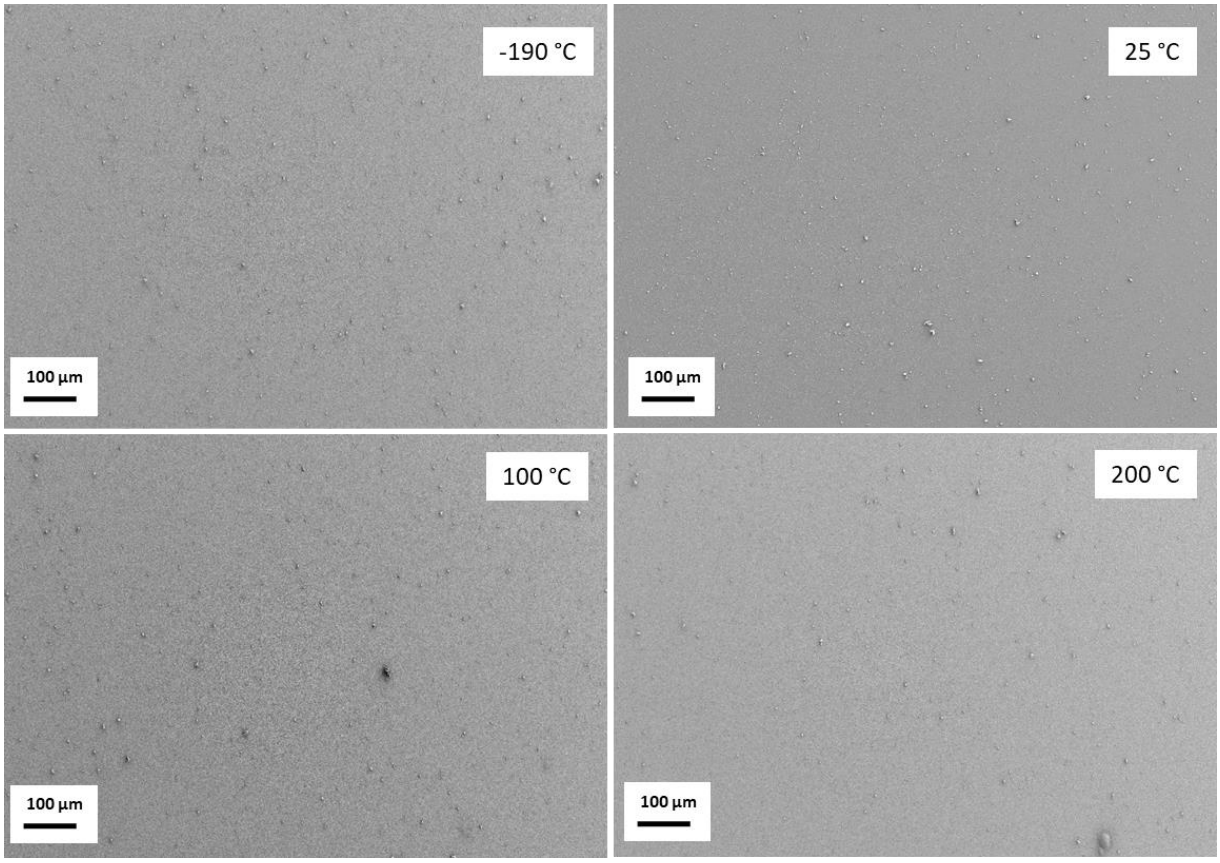

Figure 1. Scanning Electron Microscope (SEM) images of ZnO films deposited at -190, 25, 100, and 200 °C on sapphire substrates.

All ZnO samples are polycrystalline and the X-ray powder patterns exhibit the expected reflections of the wurtzite structure. In addition for the films deposited at 25 and 100 °C also weak broad reflections of metallic zinc are visible. The structural analyses in detail reveal a high disorder in the films obtained at -190 and 200 °C and a reorganization of the dioxygen ions in the middle-temperature range leading to the segregation of metallic zinc. For further details see [22].

The UV-VIS transmittance of the as-deposited ZnO films was recorded between 200 nm and 800 nm and is shown in Fig. 2 in comparison to the transmittance of the sapphire substrates used. All films show absorption edges in the UV region at approximately 380 nm with band gaps between 3.2 to 3.3 eV. The colorless films, deposited at -190 and 200 °C, are highly transparent in the visible range with an average transmittance above 90% and 95%, respectively (subtracting substrate transmittance). In contrast, the gray-yellow films obtained at 25 and 100 °C show reduced transmittances in the visible range with transmittances of 45% to 80%. Amazing is the observed transmittance after the absorption edge down to 200 nm. Normally, the transmittance of ZnO films drops rapidly to nearly zero after the edge in the range of about 50 nm. [14] For our ZnO films, this is not the case. The films show an unexpected behavior of the transmittance starting from the absorption edge at around 380 nm down to 200 nm. The decrease in transmittance (with decreasing wavelengths) ends after the edge with high transmittance values (70 to 25 %) and passes into a very slightly sloping transmittance. Full absorption is not reached up to 200 nm.

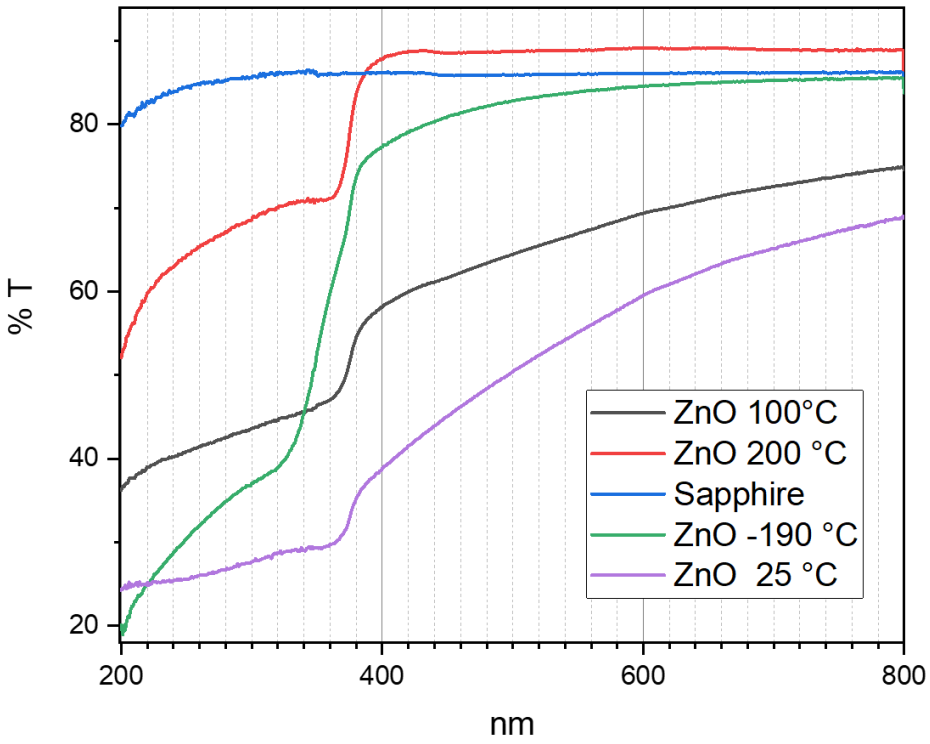

Figure 2. Transmittance (T in %) of ZnO films deposited at -190, 25, 100, and 200 °C on sapphire substrates between wavelengths of 200 and 800 nm.

Under suitable conditions, the exciton resonances are visible in ZnO films which leads to an additional absorption band at around 350 nm [15]. However, this resonance and the corresponding transmittances disappear completely at around 280 nm [15] and the excitonic phenomena cannot explain the incomplete absorption down to 200 nm. The absorption behavior of our films looks more like an

indirect band gap. One possible reason for this behavior could be the presence of dioxygen species in the ZnO films. The absorption of superoxides/peroxides has been studied for potassium and cesium superoxides (KO_2, CsO_2) as well as for hydrogen peroxide, H_2O_2. Here, sodium hydroxide solutions of hydrogen peroxide show an increasing absorption of the intramolecular electronic transition of the hydrogen peroxide anion from 300 to 200 nm [34]. The diffuse reflectance spectra of solid KO_2 and CsO_2 also show a high absorption between 500 and 200 nm with a maximum near 300 nm of the $1\pi_g \leftarrow 1\pi_u$ transition of the O_2^- ion. [35] It seems possible that similar absorption can be created by the dioxygen species (O_2^-, O_2^{2-}, …) in ZnO and are thus responsible for the observed increasing absorption from 380 to 200 nm in the measured UV/VIS spectra of our ZnO films.

This leads to the question of whether there are any indications of this behavior in the corresponding band structure. To investigate this relationship, the band structure of ideal ZnO (wurtzite structure) was calculated using a 2x2x2 supercell as well as of a relaxed ZnO structure, which contains one dioxygen species formed by moving an oxygen atom to an inverse tetrahedral void. (For full structural details see our previous work in refs [23]) Additionally, the band structure of a novel hypothetical zinc peroxide, ZnO_2, was also calculated.

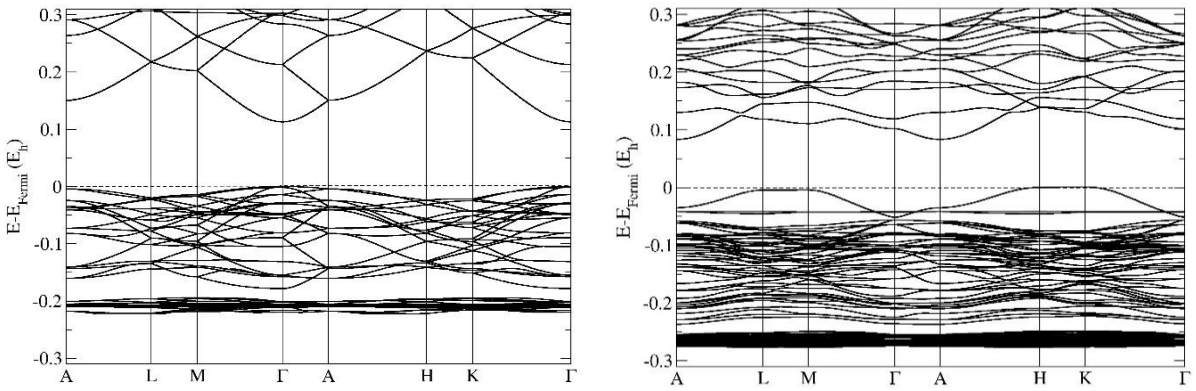

a) b)

Figure 3. The band structure of the wurtzite type is computed as: a) an ideal 2x2x2 supercell showing a direct band gap; b) a relaxed-distorted ZnO supercell structure, which contains one dioxygen species formed by moving an oxygen atom to an inverse tetrahedral void. The calculation performed using the hybrid B3LYP functional. Note that the labels of the special points of the Brillouin zones correspond to those of a hexagonal lattice.

Figure 3 shows the band structure of the wurtzite type computed as an ideal 2x2x2 supercell showing a direct band gap at the Γ-point which is comparable to the literature data. [1, 4] However, when the band structure is computed for the relaxed-distorted ZnO supercell structure, which contains one dioxygen species formed by the displacement of an oxygen atom into an inverse tetrahedral void (Figure 3b), an unusual indirect band gap has been observed. The top of the valence band (TVB) is found along the L-M and H-K directions, while the bottom of the conduction band (BCB) was found at the A-point of the Brillouin zone. In addition, the band gap was reduced from 3.08 eV ideal 2x2x2 supercell to 2.27 eV in oxygen displaced structure. We note that similar behavior was previously computed when polytypism was found in ZnO. [31]

Finally, a novel ZnO_2 compound was computed using HSE functional (here both tetrahedral voids of the wurtzite structure are filled with oxygen atoms, see Figure 4a). One notes that dioxygen species in this particular structure are very close to each other, but this structure allows a direct comparison with ZnO in the wurtzite structure. The band structure calculation of the respective ZnO_2 structure shows a direct

band gap at the Γ-point of the Brillouin zone of 3.89 eV, much closer to the equilibrium wurtzite phase (see Figure 4b). However, this type of structure offers the possibility of an indirect band gap at the TVB along the Γ-A direction of the Brillouin zone.

This study clearly illustrates the influence of the dioxygen species on the band structure and transmittance of ZnO and offers a new possibility of tuning the band gap in pure ZnO. By using different zinc oxide structure models, the anomalous behavior of the UV-VIS transmittance of the as-deposited ZnO films could be explained by an unusual behavior in the band structure and the transition between the indirect and direct band gap.

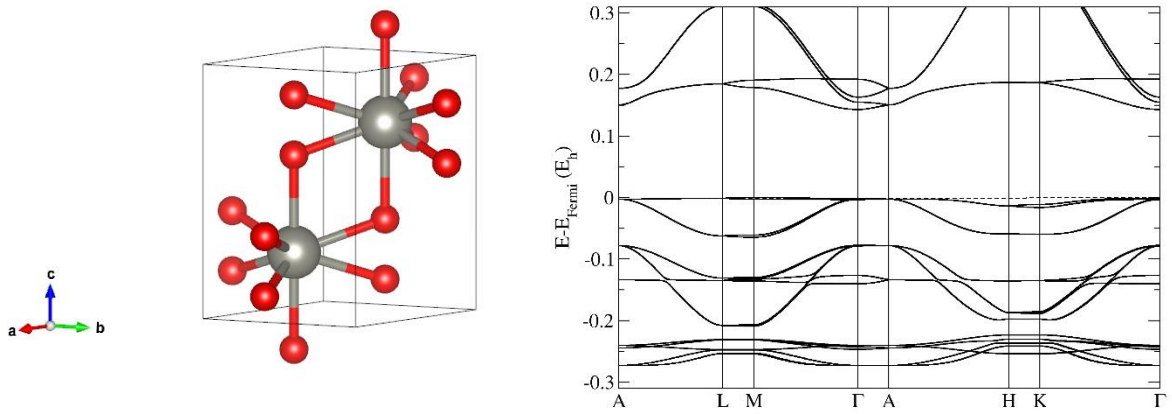

a) b)

Figure 4. a) Crystal structure of zinc peroxide, ZnO_2 computed in hexagonal space group *P*6$_3$/*mmc* (no. 194); b) corresponding band structure of the ZnO_2. The calculation performed using the hybrid B3LYP functional.

4. Conclusion

The ZnO films were deposited on sapphire substrates using the femtosecond pulsed-laser-deposition method. The deposited films are colorless at -190 and 200 °C and are gray-yellow in color at 25 and 100 °C. The gray color is caused by the segregation of zinc and the yellow color corresponds to the presence of superoxide ions and related dioxygen species in these films. The UV-VIS transmittance of the deposited ZnO films, recorded between 200 nm and 800 nm, shows an unexpected behavior of the transmittance starting from the absorption edge at around 380 nm down to 200 nm. Moreover, band structure calculations of the ZnO supercell models were performed using hybrid B3LYP functional. A novel ZnO_2 band structure was computed using HSE functional.

The observed anomalous transmittance as well as the calculated band structures support the presence of dioxygen species in the deposited ZnO films. The present study offers a new possibility of tuning the band gap in pure ZnO by employing different zinc oxide structure models and provides a possible explanation for the experimental measurements of the deposited ZnO films.

Acknowledgments

We gratefully acknowledge the helpful technical support by B. Fenk and U. Waizmann (Nanostructuring Lab) for the SEM images and Julia Kröger (Lotsch Department) for the UV/VIS measurements at the Max Planck Institute for Solid State Research. This research was also funded by the

Ministry of Science, Technological Development and Innovation of the Republic of Serbia through contract no. 451-03-47/2023-01/200017.

References

[1] Ü. Özgür, Y.I. Alivov, C. Liu, A. Teke, M.A. Reshchikov, S. Doğan, V. Avrutin, S.-J. Cho, H. Morkoç, A comprehensive review of ZnO materials and devices, Journal of Applied Physics, 98 (2005).
[2] D. Vogel, P. Krüger, J. Pollmann, Ab initio electronic-structure calculations for II-VI semiconductors using self-interaction-corrected pseudopotentials, Physical Review B, 52 (1995) R14316-R14319.
[3] S. Shabbir, A. Shaari, B. Ul Haq, R. Ahmed, M. Ahmed, Investigations of novel polymorphs of ZnO for optoelectronic applications, Optik, 206 (2020) 164285.
[4] D. Zagorac, J.C. Schön, J. Zagorac, M. Jansen, Prediction of structure candidates for zinc oxide as a function of pressure and investigation of their electronic properties, Physical Review B, 89 (2014) 075201.
[5] S. Pat, R. Mohammadigharehbagh, S. Özen, V. Şenay, H.H. Yudar, Ş. Korkmaz, The Al doping effect on the surface, optical, electrical and nanomechanical properties of the ZnO and AZO thin films prepared by RF sputtering technique, Vacuum, 141 (2017) 210-215.
[6] V. Ribić, A. Rečnik, M. Komelj, A. Kokalj, Z. Branković, M. Zlatović, G. Branković, New inversion boundary structure in Sb-doped ZnO predicted by DFT calculations and confirmed by experimental HRTEM, Acta Materialia, 199 (2020) 633-648.
[7] P. Erhart, K. Albe, A. Klein, First-principles study of intrinsic point defects in ZnO: Role of band structure, volume relaxation, and finite-size effects, Physical Review B, 73 (2006) 205203.
[8] S. Shabbir, A. Shaari, B. Ul Haq, R. Ahmed, S. AlFaify, M. Ahmed, A. Laref, First-principles investigations of electronic structures and optical spectra of wurtzite and sphalerite types of $ZnO_{1-x}S_x$ (x=0, 0.25, 0.50, 0.75 &1) alloys, Materials Science in Semiconductor Processing, 121 (2021) 105326.
[9] J. Zagorac, D. Zagorac, V. Šrot, M. Ranđelović, M. Pejić, P.A. van Aken, B. Matović, J.C. Schön, Synthesis, Characterization, and Electronic Properties of ZnO/ZnS Core/Shell Nanostructures Investigated Using a Multidisciplinary Approach, Materials, 16 (2023) 326.
[10] D. Zagorac, J. Zagorac, M. Pejić, B. Matović, J.C. Schön, Band Gap Engineering of Newly Discovered ZnO/ZnS Polytypic Nanomaterials, Nanomaterials, 12 (2022) 1595.
[11] B. Ul Haq, S. AlFaify, T. Alshahrani, R. Ahmed, F.K. Butt, S. Ur Rehman, Z. Tariq, Devising square- and hexagonal-shaped monolayers of ZnO for nanoscale electronic and optoelectronic applications, Solar Energy, 211 (2020) 920-927.
[12] B. Ul Haq, S. AlFaify, T.A. Alrebdi, R. Ahmed, S. Al-Qaisi, M.F. M. Taib, G. Naz, S. Zahra, Investigations of optoelectronic properties of novel ZnO monolayers: A first-principles study, Materials Science and Engineering: B, 265 (2021) 115043.
[13] B. Ul Haq, S. AlFaify, T. Al-shahrani, S. Al-Qaisi, R. Ahmed, A. Laref, S.A. Tahir, First-principles investigations of ZnO monolayers derived from zinc-blende and 5-5 phases for advanced thermoelectric applications, Journal of Physics and Chemistry of Solids, 149 (2021) 109780.
[14] M. Suchea, S. Christoulakis, M. Katharakis, G. Kiriakidis, N. Katsarakis, E. Koudoumas, Substrate temperature influence on the properties of nanostructured ZnO transparent ultrathin films grown by PLD, Applied Surface Science, 253 (2007) 8141-8145.
[15] J.F. Muth, R.M. Kolbas, A.K. Sharma, S. Oktyabrsky, J. Narayan, Excitonic structure and absorption coefficient measurements of ZnO single crystal epitaxial films deposited by pulsed laser deposition, Journal of Applied Physics, 85 (1999) 7884-7887.
[16] J.Y. Cho, I.K. Kim, I.O. Jung, J.-H. Moon, J.H. Kim, Effects of Mg doping concentration on the band gap of $ZnO/Mg_xZn_{1-x}O$ multilayer thin films prepared using pulsed laser deposition method, Journal of Electroceramics, 23 (2009) 442-446.
[17] D. Komaraiah, E. Radha, Y. Vijayakumar, J. Sivakumar, M. Reddy, R. Sayanna, Optical, Structural and Morphological Properties of Photocatalytic ZnO Thin Films Deposited by Pray Pyrolysis Technique. , Modern Research in Catalysis, 5 (2016) 130-146.
[18] T. Amakali, L.S. Daniel, V. Uahengo, N.Y. Dzade, N.H. de Leeuw, Structural and Optical Properties of ZnO Thin Films Prepared by Molecular Precursor and Sol–Gel Methods, Crystals, 10 (2020) 132.

[19] A. Khorsand Zak, N.S. Abd Aziz, A.M. Hashim, F. Kordi, XPS and UV–vis studies of Ga-doped zinc oxide nanoparticles synthesized by gelatin based sol-gel approach, Ceramics International, 42 (2016) 13605-13611.
[20] D. Dridi, L. Bouaziz, M. Karyaoui, Y. Litaiem, R. Chtourou, Effect of silver doping on optical and electrochemical properties of ZnO photoanode, Journal of Materials Science: Materials in Electronics, 29 (2018) 8267-8278.
[21] C. Klingshirn, B. Meyer, A. Hoffmann, J. Geurts, Zinc Oxide - From Fundamental Properties Towards Novel Applications, 2010.
[22] D. Fischer, D. Zagorac, J.C. Schön, Fundamental insight into the formation of the zinc oxide crystal structure, Thin Solid Films, 782 (2023) 140017.
[23] D. Fischer, D. Zagorac, J.C. Schön, The presence of superoxide ions and related dioxygen species in zinc oxide—A structural characterization by in situ Raman spectroscopy, J. Raman Spectrosc., 53 (2022) 2137-2146.
[24] J. C. Schön, D. Fischer, Thin films and monolayers – prediction, modeling, and experiments . Journal of Innovative Materials in Extreme Conditions, 4 (2023) 52-76.
[25] R. Dovesi, A. Erba, R. Orlando, C.M. Zicovich-Wilson, B. Civalleri, L. Maschio, M. Rérat, S. Casassa, J. Baima, S. Salustro, B. Kirtman, Quantum-mechanical condensed matter simulations with CRYSTAL, WIREs Computational Molecular Science, 8 (2018) e1360.
[26] F. Pascale, C.M. Zicovich-Wilson, F. López Gejo, B. Civalleri, R. Orlando, R. Dovesi, The calculation of the vibrational frequencies of crystalline compounds and its implementation in the CRYSTAL code, Journal of Computational Chemistry, 25 (2004) 888-897.
[27] A.D. Becke, Density-functional thermochemistry. III. The role of exact exchange, The Journal of Chemical Physics, 98 (1993) 5648-5652.
[28] J. Heyd, G.E. Scuseria, M. Ernzerhof, Hybrid functionals based on a screened Coulomb potential, The Journal of Chemical Physics, 118 (2003) 8207-8215.
[29] Tamara Škundrić, Branko Matović, Aleksandra Zarubica, Dorota Chudoba, D. Zagorac, Data mining ab initio study of gypsum and $CaCO_3$ modifications at standard and extreme conditions, Journal of Innovative Materials in Extreme Conditions, 4 (2023) 38-51.
[30] Milan Pejić, Dejan Zagorac, Jelena Zagorac, Tamara Škundrić, B. Matović, Theoretical study of ground state properties of Na^+, Cs^+, Mg^{2+} and Ba^{2+} doped mayenite and its electride forms under extreme conditions, Journal of Innovative Materials in Extreme Conditions, 3 (2022) 30-42.
[31] D. Zagorac, J.C. Schön, J. Zagorac, M. Jansen, Theoretical investigations of novel zinc oxide polytypes and in-depth study of their electronic properties, RSC Advances, 5 (2015) 25929-25935.
[32] R. Hundt, KPLOT, A Program for Plotting and Analyzing Crystal Structures, Technicum Scientific Publishing, Stuttgart, Germany, 2016.
[33] K. Momma, F. Izumi, VESTA: a three-dimensional visualization system for electronic and structural analysis, J. Appl. Crystallogr., 41 (2008) 653-658.
[34] J. Chlistunoff, J.-P. Simonin, Ionic Association of Hydroperoxide Anion HO_2^- in the Binding Mean Spherical Approximation. Spectroscopic Study of Hydrogen Peroxide in Concentrated Sodium Hydroxide Solutions, J. Phys. Chem. A, 110 (2006) 13868-13876.
[35] S.A. Hunter-Saphir, J.A. Creighton, Resonance Raman scattering from the superoxide ion, J. Raman Spectrosc., 29 (1998) 417-419.